Araştırma Makalesi / Research Article

Similarity Solutions of a non-Newtonian Fluid's Momentum and Thermal Boundary Layers: Cross Fluid Model

Hikmet SÜMER[1], Yiğit AKSOY[2]

[1,2] *Celal Bayar University, Faculty of Engineering, Mechanical Engineering Department, Manisa.*

Corresponding author e-mail: ygtaksoy@gmail.com   ORCID ID: http://orcid.org/0000-0002-4613-4042
sumerhikmet@gmail.com ORCID ID: http://orcid.org/0000-0001-7830-0044

Abstract

The steady, incompressible and laminer flow of a non-Newtonian fluid that fits the Cross-fluid model over a flat plate is investigated. Dimensionless momentum and energy equations in partial differential form are derived to examine the variation of fluid velocity and temperature. The equations are simplified by the boundary layer theory based on the assumption that the change occurs in a narrow region, then scaling symmetries are calculated. By means of symmetries, equations in a partial form are reduced to an ordinary form by computing similarity variables and functions. The sbvp2.0 package developed for the Matlab environment based on collocation methods was used for the numerical solutions of the equations. In the light of analytical approach and solutions, the heat transfer is investigated by the Nusselt number. The study reveals that increases in Weissenberg number and power-law index, as non-Newtonian properties, are in charge of the thinner boundary layers, thus causing less friction and effective convection. As a result of numerical parts of the study, sbvp2.0 package is recomended for stiff equations with high nonlinearity, especially arising from boundary layer flows.

Bir Newtonyen Olmayan Akışkanın Momentum ve Isıl Sınır Tabakalarının Benzerlik Çözümleri: Cross Akışkan Modeli

Öz

Bu çalışma kapsamında Newtonyen olmayan Cross akışkanının sabit bir plaka üzerinde sıkıştırılamaz laminer akışı incelenmiştir. Kısmi diferansiyel denklem formundaki boyutsuz momentum ve enerji denklemleri çözümlenerek akışkanın hızı ve sıcaklık değişimleri incelenmiştir. Bu denklemler akışkan hız ve sıcaklık değişiminin dar bir bölgede gerçekleştiği varsayımına dayanan sınır tabakası teorisi ile sadeleştirilmiştir. Sınır tabakası denklemlerinin simetrileri ölçekleme dönüşüm formülleri ile tespit edilip, bu simetriler yardımıyla benzerlik değişkenleri ve fonksiyonlar kullanılarak, kısmi diferansiyel denklemlerin eşdeğer adi diferansiyel denklemleri bulunmuştur. Denklemlerin sayısal çözümleri için, sıralama noktalarını kullanarak denklemlerin nümerik çözümlerini bulmayı sağlayan Matlab ortamı için geliştirilen sbvp2.0 paketi kullanılmıştır. Analitik yaklaşım ve çözümler ışığıyla akışkanın ısı transferi Nusselt sayısı ile incelenmiştir. Artan Weissenberg sayısı ve power-law indeksi ile sınır tabakalarının kalınlaştığı ve bu sayede daha az sürtünme ve etkili konveksiyona sebep olduğu çalışmadan bulunmuştur. Çalışmanın sayısal kısmının sonucu olarak sbvp2.0 paketi yüksek doğrusal olmayan davranışa sahip özellikle sınır tabakası akışlarından ortaya çıkmış denklemler için önerilmektedir.

1. Introduction

The linear relationship between the applied shear stress and the deformation rate of the fluid indicates the constant viscosity and the fluids displaying this behaviour are called "Newtonian fluid". However, while Newtonian fluids are always viscous fluids with a viscosity, not all viscous fluids may be Newtonian, i.e., non-Newtonian fluids. Although the definition of non- Newtonian is mostly perceived as

variable viscosity, many properties such as viscoelasticity and deformation memory, i.e., thixotropy, etc., that are separated from the Newtonian fluid are studied by Rheology. Nevertheless, in most non-Newtonian fluid problems, especially this study, which are related to science and engineering, only the acceptance of viscosity that varies with deformation rate is sufficient. Fluids in which viscosity changes with deformation rate obey the following "generalized Newtonian fluid (GNA)" (Morrison 2001), shear stress strain rate relationship.

$$\boldsymbol{\tau} = \eta\left(|\dot{\boldsymbol{\gamma}}|\right)\dot{\boldsymbol{\gamma}} \tag{1}$$

Here $\boldsymbol{\tau}$ and $\dot{\boldsymbol{\gamma}}$ are tensors containing shear stresses and strain rates in all directions, respectively. Also, by definition, the viscosity function or apparent viscosity η is the function of the norm of the deformation tensor, i.e., $|\dot{\boldsymbol{\gamma}}|$. In the expression above, it corresponds to the Newtonian fluid state of the case where $\eta = constant$. Fluids that comply with this definition we observe in nature and have increased viscosity with increasing deformation speed are called shear thickening fluids, on the contrary, those with decreasing viscosity are called shear thinning fluids. The increase or decrease in viscosity with increasing deformation rate encountered here can be predicted by the power-law formula, a generalized Newtonian fluid model (Wan Nik *et al.* 2005):

$$\eta\left(|\dot{\boldsymbol{\gamma}}|\right) = \kappa|\dot{\boldsymbol{\gamma}}|^{n-1} \tag{2}$$

where κ is the fluid parameter and n is the power-law index. For swelling fluids, i.e., $n > 1$, as the deformation rate increases, i.e., $\dot{\boldsymbol{\gamma}} \to \infty$, the apparent viscosity η of the fluid will increase and the fluid will become more viscous. In shear thinning fluids, i.e., $0 < n < 1$, apparent viscosity will decrease as the deformation rate increases. Note that while the deformation rate increases in the power-law fluid model, the apparent viscosity increases or decreases depending on whether the fluid is shear thinning or swelling. However, with few exceptions (Galindo-Rosales *et al.* 2011) in reality most fluids have a constant initial viscosity η_0 at low deformation rates, i.e., $\dot{\boldsymbol{\gamma}} \sim 0$, as can be seen

from Figure (1). After the critical deformation rate is exceeded, the fluid enters the power-law region where its viscosity changes and at high deformation rates it has a permanent η_∞ limit viscosity value. Although most thinning and swelling fluids react to increasing deformation rates in the opposite ways, these three different regions are seen in the experimental viscosity-strain rate graphs where the power-law formula cannot predict plateau regions. For example, for shear thinning fluids, in case of $\dot{\boldsymbol{\gamma}} \sim 0$, the deformation rate will be the denominator in the formula, so the power-law formula will give an unrealistic rather high apparent viscosity value. Similarly, in the case of $\dot{\boldsymbol{\gamma}} \to \infty$, it can be said that the viscosity converges to zero in thinning fluids and to infinity in swelling fluids. However, in reality the viscosity of a fluid can be neither zero nor infinite. As a result, although the power-law formula gives quite acceptable results in a wide range of deformation rates, it is not useful at very low and high deformation rates. Various models have been developed by researchers that can predict end regions where viscosity does not change where the power-law model fails, while providing the transient zone (Raju *et al.* 1993). Models of this type that try to predict a more complex behaviour are computationally more laborious and require considerably more parameters than the power-law and Newtonian models. One of the best known of these models is the Cross-fluid model below, which is highly available for most thinning fluids (Cross 1965).

$$\eta\left(|\dot{\boldsymbol{\gamma}}|\right) = \eta_\infty + \frac{\eta_0 - \eta_\infty}{1 + \lambda|\dot{\boldsymbol{\gamma}}|^n} \tag{3}$$

Here λ is the strain rate multiplier for the Cross-fluid model. If you pay attention, unlike the power-law model given in Equation (2), the initial and limit viscosity values are found in the above formula as η_0 and η_∞, respectively. Limit viscosity η_∞ for shear thinning fluids is considerably smaller than the initial viscosity η_0, shortly $\eta_0 \gg \eta_\infty$. In addition, to reach the limit viscosity value, i.e., $|\dot{\boldsymbol{\gamma}}| \to \eta_\infty$, high deformation rates, $\lambda|\dot{\boldsymbol{\gamma}}| \gg 1$ are required. For these results, the simplified Sisko fluid model (Sisko 1958) below is preferred instead of the Cross-fluid model, except for low deformation rates.

$$\eta\left(|\dot{\gamma}|\right) = \eta_\infty + \frac{\eta_0}{\lambda |\dot{\gamma}|^n} \tag{4}$$

However, unlike power-law and Sisko fluid, if a model that will provide all the regions in Figure (1) is sought, the Cross formula should be preferred. In addition, fluid models of Carreau (Bird 1976), Carreau-Yassuda (Yasuda *et al*. 1981), Williamson (Williamson 1929) and Philippoff (Na 1994), which have more than one parameter to be alternative to the Cross-fluid model, can be used for GNA analysis. Besides shear stress depending on the only shear stress, fluid might exhibit a viscoelastic property that GNA models cannot capture. Instead, many constitutive equations predict such responses to external stimuli; from literature, Burger's model (Javaid *et al*. 2022), Maxwell fluid (Riaz *et al*. 2021), second-grade fluid (Riaz 2021), Walters'-B fluid (Sunthrayuth 2021), and fractional second-grade fluid (Javed *et al*. 2021, Iftikhar 2021).

In this study, the flow of a viscous fluid on a flat plate will be discussed in the Cross formula. Fluid at uniform velocity and constant temperature has a variable velocity profile in a very narrow area close to the plate after it contacts the planar stationary plate and reaches uniform velocity again as it moves away from the plate. Also, while the plate is kept at a constant temperature, a similar change is observed in the temperature of the fluid. The fact that the variations are stuck in a narrow region makes it unnecessary to examine the entire flow region. In light of this idea, the boundary layer theory, in which some of the physical changes are hierarchically ignored, was developed to analyse only a narrow region (Schlichting and Gersten 2017). This theory is based on a systematic simplification approach for the executive equations valid in the region in question and helps to derive boundary layer equations that are easier to handle mathematically. In the case of Newtonian flows of this type, simplified forms using this theory instead of Navier-Stokes equations, i.e., Newtonian momentum boundary layer equations are generally preferred. In addition, boundary layer assumptions apply to momentum equations and, in some cases, to energy and concentration equations that need to

be solved as conjugate and other boundary layer equations related to non-momentum conservation laws can also be obtained. As the momentum equations of non-Newtonian fluids can be of higher order than the Navier-Stokes equations, they contain both more terms and more nonlinear interactions between these terms, so simplifying mathematical tools such as boundary layer and perturbation theory are frequently used in analyses. For example, Aksoy *et al*. applied the boundary layer theory to viscoelastic Oldroyd and Maxwell (Pakdemirli *et al*. 2013, Değer *et al*. 2011), second-order fluid with viscoelastic and power-law properties (Aksoy *et al*. 2007, Pakdemirli *et al*. 2008), Sisko (Sarı *et al*. 2012), Williamson (Aksoy *et al*. 2012), Powell-Eyring (Hayat *et al*. 2013) models as GNA and various flow types were investigated. In this study, momentum and thermal boundary layer equations of Cross-fluid will be shared with the literature for the first time and numerical solutions for laminar flow on the plate will be presented. The variations of dimensionless fluid velocity and temperature obtained from numerical solutions of boundary layer equations according to the Weissenberg number, Prandtl number and power-law index will be observed on the graphs. In addition to the shear stress applied by the fluid to the plate, a qualitative analysis of the heat transfers between the plate and the fluid over the Nusselt number was carried out.

2. Problem Statement and Governing Equations

2.1 Physical Construction

In Figure (2), the behaviour of the incompressible fluid at T_∞^* temperature coming with uniform U_∞^* velocity after touching the stationary planar rigid plate of length L is represented. According to the figure, let us take any point x_i^* on the plate and examine how the x^* component of the two-dimensional fluid velocity $u_i^*(x_i^*, y^*)$ changes in the vertical direction. After the velocity of the first fluid layer u_0^* contacts the plate, it is reset due to the non-slip condition, i.e., $u_0^* = 0$. However, due to the effect of only relatively low viscous forces relative to the solid surface interaction, the first fluid layer in the vertical direction adjacent to this layer will have

a relative velocity u_1^*, i.e., $u_1^* > 0$. Similarly, for a fixed point y_i^* the velocity of the fluid plates continues to increase until a certain point y_i^* in the vertical direction, the freestream velocity continues to increase up to U_∞^*, i.e., $u_i^*(x_i^*, y^* \to y_i^*) \to U_\infty^*$. Now consider the point x_{i+1}^* on the plate. At this point, the fluid velocity in the vertical direction, or the fluid velocity profile, u_{i+1}^* changes similarly, but at a higher point in the vertical direction, i.e., $y_{i+1}^* > y_i^*$, the velocity of fluid layers reaches U_∞^*. Therefore, the fluid will have different velocity profiles at the x_i^* and x_{i+1}^* point and the change in these velocity profiles will continue until a certain point x_∞^*. From this point on, the x^* component of the fluid's velocity u^* loses its change in two dimensions and is said to change only in the y^* direction, i.e., $u^*(x^* \to x_\infty^*, y^*) = u_\infty^*(y^*)$. The resulting $\delta^*(x^*)$ curve when we connect all these y_i^* points on the plate is called the boundary layer. Note that the fluid velocity is constant and U_∞^* at each point in the region above the boundary layer curve. Experimental studies using streamline visualization techniques have shown that this region between the boundary layer and the plate where the fluid velocity varies is quite narrow, i.e., $\delta^*(x^*) \ll 1$. The very small acceptance in question is the most important building block of the boundary layer theory, which we will make next. As we will see in future analysis, the theory is based on determining the ranges of the elements of the speed, temperature functions and coordinate system that constitute all the executive equations according to the nature of the problem according to the boundary layer thickness $\delta^*(x^*)$ and neglecting small terms relative to each other. Although the relationship with the conservation of momentum is the velocity boundary layer we visualized in this section, it can likewise be drawn in the thermal boundary layer. Starting from the plate temperature T_0^*, the fluid temperature inside the thermal boundary layer will catch the free stream temperature T_∞^* at a certain height.

2.2 Equation of Momentum

If Newton's second law is applied to a very small incompressible viscous fluid particle with steady and laminar flow acceptance, the following vector momentum equation, independent of the coordinate system, is obtained.

$$\rho \, \mathbf{v}.\nabla \mathbf{v} = -\nabla P^* - \nabla.\boldsymbol{\tau} \tag{5}$$

Here ρ is the fluid density, $\mathbf{v} = u \, \mathbf{e_1} + v \, \mathbf{e_2}$ is the velocity vector containing velocity components in all directions, ∇P^* pressure gradient and $\boldsymbol{\tau}$ is the fluid type-dependent shear stress tensor. In addition, the fluid velocity vector must satisfy the continuity equation valid for the following incompressible fluids, due to the conservation of matter.

$$\nabla.\mathbf{v} = 0 \tag{6}$$

The vectorial momentum equation given by Equation (5) for two-dimensional Cartesian coordinates can be written as:

$$\rho\left(u^* \frac{\partial u^*}{\partial X^*} + v^* \frac{\partial u^*}{\partial Y^*}\right) = \frac{\partial P^*}{\partial X^*} + \frac{\partial}{\partial X^*}\tau_{X^*X^*} + \frac{\partial}{\partial Y^*}\tau_{X^*Y^*}$$
$$\rho\left(u^* \frac{\partial v^*}{\partial X^*} + v^* \frac{\partial v^*}{\partial Y^*}\right) = \frac{\partial P^*}{\partial Y^*} + \frac{\partial}{\partial X^*}\tau_{X^*Y^*} + \frac{\partial}{\partial Y^*}\tau_{Y^*Y^*} \tag{7}$$

Continuity equation is as follows:

$$\frac{\partial u^*}{\partial X^*} + \frac{\partial v^*}{\partial Y^*} = 0 \tag{8}$$

Equation (7-8) is the general equation of velocity field in cartesian coordinates for incompressible, laminer and steady flows, and is independent of the fluid model. For the studied fluids, based on the generalization of $\eta_0 \gg \eta_\infty$ we mentioned earlier, ignoring the η_∞ and calculating the shear stresses in Equation (7) from Equation (3) as follows.

$$\tau_{X^*X^*} = 2\left[\mu_0\left(1 + \lambda\left(2\left(\frac{\partial u^*}{\partial X^*}\right)^2 + 2\left(\frac{\partial v^*}{\partial Y^*}\right)^2 + \left(\frac{\partial u^*}{\partial Y^*} + \frac{\partial v^*}{\partial X^*}\right)^2\right)^{\frac{n}{2}}\right)^{-1}\right]\frac{\partial u^*}{\partial X^*}$$

$$\tau_{X^*Y^*} = \left[\mu_0\left(1 + \lambda\left(2\left(\frac{\partial u^*}{\partial X^*}\right)^2 + 2\left(\frac{\partial v^*}{\partial Y^*}\right)^2 + \left(\frac{\partial u^*}{\partial Y^*} + \frac{\partial v^*}{\partial X^*}\right)^2\right)^{\frac{n}{2}}\right)^{-1}\right]\left(\frac{\partial v^*}{\partial X^*} + \frac{\partial u^*}{\partial Y^*}\right) \tag{9}$$

$$\tau_{Y^*Y^*} = 2\left[\mu_0\left(1 + \lambda\left(2\left(\frac{\partial u^*}{\partial X^*}\right)^2 + 2\left(\frac{\partial v^*}{\partial Y^*}\right)^2 + \left(\frac{\partial u^*}{\partial Y^*} + \frac{\partial v^*}{\partial X^*}\right)^2\right)^{\frac{n}{2}}\right)^{-1}\right]\frac{\partial v^*}{\partial Y^*}$$

It should be said here that $\tau_{X^*Y^*} = \tau_{Y^*X^*}$ since the shear stress tensor is symmetrical. If the above shear stresses are placed in Equation (7), momentum equations in Cartesian coordinates are obtained for the Cross fluid. Simplifying

assumptions can be applied to momentum equations that we will not derive in this study, and momentum boundary layer equations can be obtained. However, instead of this, we will obtain the boundary layer equation from Equations (7) and (9), which we think are easier, with the assumptions applied.

2.3 Equation of Energy

The two-dimensional steady state energy equation with neglected viscous heating effects for any fluid mass in Cartesian coordinates can be written as:

$$u^* \frac{\partial T^*}{\partial X^*} + v^* \frac{\partial T^*}{\partial Y^*} = \frac{k}{\rho c_p} \left(\frac{\partial^2 T^*}{\partial X^{*2}} + \frac{\partial^2 T^*}{\partial Y^{*2}} \right) \tag{10}$$

Here k is the thermal conductivity, ρ is the density and c_p is the specific heat of the fluid. In the next section, the boundary layer assumptions will be applied directly to the energy equation as it contains much less terms than the momentum equation. Although we have made a physical definition of our problem so far, we have not defined our boundary conditions since we have not yet presented the momentum and thermal boundary layer equations that we will solve numerically. This topic will be discussed in the section of boundary layer equations.

3. Boundary Layer Assumptions

Based on experimental observations in previous sections, it was stated that the boundary layer thickness is a very small size, i.e., $\delta^* \ll 1$. Considering that the forces of the terms smaller than one are listed as $\delta^{*3} \ll \delta^{*2} \ll \delta^* \ll 1 \ll 1/\delta^{*2} \ll 1/\delta^{*3}$, let us determine the orders of velocity, coordinate components and temperature in the problem, in other words, what $O(\delta^*)$ their magnitudes are around. First of all, compared to the L plate length δ^* is quite small. Therefore, we can say that it is on the order of 1 for L, i.e., $L \sim O(1)$. If the horizontal component of the coordinate system is x^*, it must be of the same magnitude, i.e., order of 1, since it can represent every point on L, i.e., $x^* \sim O(1)$. A similar relation should be between vertical coordinate y^* and

boundary layer thickness δ^* as in the relation of order of horizontal axis x^* and plate length L. Since we will only examine the inside of the boundary layer, the maximum value that the values of the vertical y^* coordinate can take will be δ^*, i.e., $y^* \sim O(\delta^*)$. If the vertical velocity is u^*, the order of 1 can be accepted as it is the velocity across the plate, i.e., $u^* \sim O(1)$. When we look at our continuity equation given by Equation (8), we should say that the terms $\partial u^*/\partial x^*$ and $\partial v^*/\partial y^*$ must be of the same order. This is because, due to the conservation of mass, the change in one term with a reverse sign must be observed in the other term ,i.e., from Equation (8) $\partial u^*/\partial x^* = -\partial v^*/\partial y^*$. Since the order of u^* and x^* in the first term is 1, it is obvious that $\partial u^*/\partial x^*$ must also have order 1, i.e., $\partial u^*/\partial x^* \sim O(1)$. Therefore, since $\partial v^*/\partial y^* \sim O(1)$ and $y^* \sim O(\delta^*)$, vertical velocity will be a term of order v^*, δ^*, i.e., $v^* \sim O(\delta^*)$. Since the temperature must take a value outside of the boundary layer, there is no reason for us not to accept that it is on the order of 1, i.e., $T^* \sim O(1)$. In summary, the orders of the fundamental magnitudes are given in the form:

$$u^*, x^* \text{ ve } T^* \sim O(1),$$
$$v^* \text{ ve } y^* \sim O(\delta^*). \tag{11}$$

The application of boundary layer assumptions to equations consists in systematically deciding on small terms according to their order and neglecting them compared to large terms. For example, let us state the order of each term in the first $\tau_{X^*Y^*}$ from the shear stress given by Equation (9) as follows.

$$\tau_{X^*Y^*} = \left\{ \mu_0 \left[1 + \lambda \left[2 \underbrace{\left(\frac{\partial u^*}{\partial X^*} \right)^2}_{O(1)} + 2 \underbrace{\left(\frac{\partial v^*}{\partial Y^*} \right)^2}_{O(1)} + \left(\underbrace{\frac{\partial u^*}{\partial Y^*}}_{O\left(\frac{1}{\delta^*}\right)} + \underbrace{\frac{\partial v^*}{\partial X^*}}_{O(\delta^*)} \right)^2 \right]^{\frac{n}{2}} \right]^{-1} \right\} \left(\underbrace{\frac{\partial v^*}{\partial X^*}}_{O(\delta^*)} + \underbrace{\frac{\partial u^*}{\partial Y^*}}_{O\left(\frac{1}{\delta^*}\right)} \right) \tag{12}$$

First of all, let's say that the terms should be in the same parenthesis, that is, they should not be in multiplication with each other in order to be compared with each other. Therefore, the highest order term $(\partial u^*/\partial y^*)^2 \sim O(1/\delta^{*2})$ is kept in the inner parentheses and other terms are ignored. Similarly, if the term $\partial u^*/\partial y^* \sim O(1/\delta^*)$ in the

outermost parenthesis is kept and the equation is edited, with

$$\tau_{x^*y^*} = \eta_0 \left(1 + \lambda \left(\frac{\partial u^*}{\partial y^*}\right)^n\right)^{-1} \frac{\partial u^*}{\partial y^*}$$
(13)

the shear stress $\tau_{X^*Y^*}$ valid within the boundary layer is reached. After applying the same assumptions, the remaining statements from Equation (9) are as follows.

$$\tau_{x^*x^*} = 2\eta_0 \left(1 + \lambda \left(\frac{\partial u^*}{\partial y^*}\right)^n\right)^{-1} \frac{\partial u^*}{\partial x^*}$$

$$\tau_{y^*y^*} = 2\eta_0 \left(1 + \lambda \left(\frac{\partial u^*}{\partial y^*}\right)^n\right)^{-1} \frac{\partial v^*}{\partial y^*}$$
(14)

Since we do not have any information about the orders of η_0 and λ in the above statement, the simplest expressions of shear stresses are like these. Likewise, our momentum equation in the x^* direction simplifies to the following figure with the assumption that the shear stresses are of the same order.

$$\rho\left(u^*\frac{\partial u^*}{\partial x^*} + v^*\frac{\partial u^*}{\partial y^*}\right) = \frac{\partial P^*}{\partial x^*} + \frac{\partial}{\partial y^*}\tau_{x^*y^*}$$
(15)

The $\tau_{x^*y^*}$ given in Equation (14) is placed in the above expression and after some arrangements it is written with the degrees of each term as:

$$\rho\left(\underbrace{u^*\frac{\partial u^*}{\partial x^*} + v^*\frac{\partial u^*}{\partial y^*}}_{o(1)}\right) = \underbrace{-\frac{\partial P^*}{\partial x^*}}_{o(1)} + \underbrace{\eta_0 \frac{\partial^2 u^*}{\partial y^{*2}}}_{o\left(\frac{1}{\delta^2}\right)} \left(\frac{1 - n\lambda\left|\frac{\partial u^*}{\partial y^*}\right|^n\left(1 + \lambda\left|\frac{\partial u^*}{\partial y^*}\right|^n\right)^{-1}}{\underbrace{1 + \lambda\left|\frac{\partial u^*}{\partial y^*}\right|^n}_{o(\delta)}}\right)_{o\left(\frac{1}{\delta}\right)}$$
(16)

In the above statement, the terms on the left are on the order of 1, but are expressions of the acceleration of the fluid particle coming from Newton's second law. In order for these expressions to be balanced with the expressions related to pressure and viscous forces on the right side, $\eta_0 \sim O(\delta^2)$ and $\lambda \sim O(\delta)$ must be respectively when $P^* \sim O(1)$. By calculating the orders of all boundary layer magnitudes up to here, y^* momentum equation is reduced to the following simple form.

$$\frac{\partial P^*}{\partial y^*} = 0$$
(17)

From here it can be seen that $P^* = P^*(x)$. In addition, since the fluid outside the boundary layer has a uniform velocity, the following expression is calculated from the Bernoulli equation with the potential flow assumption.

$$P^* = -\frac{1}{2}U_\infty^{*2} + \text{constant}$$
(18)

When we take the derivative of the above expression once, the pressure gradient in Equation (16) is found as follows.

$$\frac{dP^*}{dx^*} = -U_\infty^* \frac{dU_\infty^*}{dx^*}$$
(19)

In addition, the boundary conditions suitable for the physical configuration of the problem are as follows:

$$u^*(x^*,0) = v^*(x^*,0) = 0, \; u^*(x^*,\infty) = U_\infty^* \text{ and } \frac{\partial u^*}{\partial y^*}(x^*,\infty) = 0.$$
(20)

Similarly, the energy equation given by Equation (10) is reduced to the following thermal boundary layer equation.

$$u^*\frac{\partial T^*}{\partial x^*} + v^*\frac{\partial T^*}{\partial y^*} = \frac{k}{\rho c_p}\frac{\partial^2 T^*}{\partial y^{*2}}$$
(21)

The appropriate boundary conditions are as follows.

$$T^*\left(x^*,0\right) = T_w^* \text{ and } T^*(x^*,\infty) = T_\infty^*.$$
(22)

Let us propose the following new dimensionless variables for the boundary layer equations and boundary conditions that we have derived.

$$u = \frac{u^*}{V}, v = \sqrt{Re}\frac{v^*}{V}, x = \frac{x^*}{L}, y = \sqrt{Re}\frac{y^*}{L}, P = \frac{P^*}{\rho V^2}, U_\infty = \frac{U_\infty^*}{V} \text{ and } T = \frac{T^*-T_\infty^*}{T_w^*-T_\infty^*}$$
(23)

Here $Re = \rho V L / \eta_0$ is the Reynolds number and V is the reference speed. In order to emphasize the power-law effect in the equations, the dimensionless momentum boundary layer equation and related boundary conditions are obtained as follows after the $\bar{\lambda}^m = \lambda$ transformation;

$$\left(u\frac{\partial u}{\partial x}+v\frac{\partial u}{\partial y}\right)=U_\infty\frac{dU_\infty}{dx^*}+\frac{\partial^2 u}{\partial y^2}\left(\frac{1-n\left|Wi\frac{\partial u}{\partial y}\right|^n\left(1+\left|Wi\frac{\partial u}{\partial y}\right|^n\right)^{-1}}{1+\left|Wi\frac{\partial u}{\partial y}\right|^n}\right),\quad (24)$$

$$u(x,0)=v(x,0)=0,\ u(x,\infty)=U_\infty\ \text{and}\ \frac{\partial u}{\partial y}(x,\infty)=0$$

where $Wi=\sqrt{\rho VL/\eta_0}\ \bar\lambda V/L$ is the Weissenberg number representing the ratio of elastic forces to viscous forces. Also note that the resulting Weissenberg number is equal to the product of the Deborah number $De=\bar\lambda V/L$ and $\sqrt{Re}$, i.e., $Wi=\sqrt{Re}\ De$. For non-Newtonian fluids, the ratio of the time taken for the applied shear stress to be completely damped in the fluid and any characteristic time in the system gives the well-known dimensionless time Deborah number. Accordingly, it can be said that the behaviour of a non-Newtonian fluid with a high Deborah number will be closer to a solid matter, or vice versa, for low Deborah numbers the matter will be more fluid. Our dimensionless continuity equation that needs to be solved with the momentum equation to obtain velocity profiles becomes

$$\frac{\partial u}{\partial x}+\frac{\partial v}{\partial y}=0 \qquad (25)$$

The energy equation and boundary conditions are as follows.

$$u\frac{\partial T}{\partial x}+v\frac{\partial T}{\partial y}=\mathrm{Pr}^{-1}\frac{\partial^2 T}{\partial Y^2}, \qquad (26)$$

$$T(x,0)=1\ \text{and}\ T(x,\infty)=0$$

Here $Pr=\rho c_p/k$ is the Prandtl number and is the ratio of momentum diffusivity to thermal diffusivity in the fluid, or, as we are concerned, the ratio of momentum boundary layer thickness to thermal boundary layer thickness. In order to eliminate the continuity equation, let us write the fluid velocities in terms of stream functions $u=\partial\Psi/\partial y$ and $v=\partial\Psi/\partial x$. Our momentum boundary layer equation and conditions in terms of stream functions using subscript notation for derivatives reduced to:

$$\left(\Psi_y\Psi_{xy}-\Psi_x\Psi_{yy}\right)=U_\infty\frac{dU_\infty}{dx^*}+\Psi_{yyy}\left(\frac{1-\left|Wi\,\Psi_{yy}\right|^n\left(1+\left|Wi\,\Psi_{yy}\right|^n\right)^{-1}}{1+\left|Wi\,\Psi_{yy}\right|^n}\right), \quad (27)$$

$$\Psi_y(x,0)=0,\ \Psi_y(x,\infty)=U_\infty,\ \Psi_x(x,0)=0,\ and\ \Psi_{yy}(x,\infty)=0$$

Our thermal boundary layer equation and conditions reduced to

$$\Psi_y T_x-\Psi_x T_y=\mathrm{Pr}^{-1}T_{yy}, \qquad (28)$$

$$T(x,0)=1\ \text{and}\ T(x,\infty)=0$$

Equations (27) and (28) are boundary layer equations in partial differential form, which we will try to reduce to ordinary form with similarity transformations for numerical solutions in the following sections. Although ready-made transformations are frequently used in the literature for similarity transformations, in this study we will refer to special transformations obtained by using the symmetries of the equations.

4. Symmetry Analysis

If the equation does not change when some special transformations are applied to the variables of an equation, these transformations are called the symmetries of the equation. Lie group theory (Bluman and Kumei 2013) deals with all the symmetries that a differential equation has. With the systematic approach of Lie group theory, all symmetries of a differential equation can be found. If the equation dealt with by the symmetries found is ordinary differential equation, it is reduced to the canonical form and the solution is found, if it is a partial differential equation, it can also be reduced to ordinary form. In studies investigating all the symmetries accepted by the equations using Lie algebra, it has been observed that the boundary layer equations generally remain invariant under scaling transformations. Therefore, instead of a general analysis, we will calculate the scaling transformation that our boundary layer equations accept. First, let us define our new variables scaled with the following uncertain parameters as follows

$$\Psi=e^{\varepsilon\alpha_1}\overline\Psi,\ x=e^{\varepsilon\alpha_2}\overline x,\ y=e^{\varepsilon\alpha_3}\overline y,\ U_\infty=e^{\varepsilon\alpha_4}\overline U_\infty,\ T=e^{\varepsilon\alpha_5}\overline T \quad (29)$$

in which ε is a small parameter. By ignoring the accents, in terms of these variables Equation (19) takes this form:

$$\left(\Psi_y\Psi_{xy}-\Psi_x\Psi_{yy}\right)=e^{2\alpha_1-2\alpha_2+2\alpha_3}U_\infty\frac{dU_\infty}{dx^*}+e^{-\alpha_1-\alpha_3+\alpha_2}\Psi_{yyy}\left(\frac{1-\left|e^{\alpha_1-2\alpha_3}Wi\,\Psi_{yy}\right|^n\left(1+\left|e^{\alpha_1-2\alpha_3}Wi\,\Psi_{yy}\right|^n\right)^{-1}}{1+\left|e^{\alpha_1-2\alpha_3}Wi\,\Psi_{yy}\right|^n}\right) \quad (30)$$

where Equation (26) takes this form:

$$\Psi_y T_x - \Psi_x T_y = \Pr^{-1} e^{-\alpha_1 + \alpha_2 - \alpha_3} T_{yy}, \tag{31}$$

Under these transformations, for Equations (30) and (31) to be the same as (27) and (28), exponential functions must be equal to 1, so these algebraic equations are written:

$$\begin{aligned} -2\alpha_1 + 2\alpha_3 + 2\alpha_5 &= 0 \\ -\alpha_1 + \alpha_2 - \alpha_3 &= 0 \\ \alpha_1 - 2\alpha_3 &= 0 \end{aligned} \tag{32}$$

The solution of the equation system α_4 is arbitrary, the value is taken as c and all other unknowns are found in terms of α_3 as follows:

$$\begin{bmatrix} \alpha_1 \\ \alpha_2 \\ \alpha_3 \\ \alpha_4 \\ \alpha_5 \end{bmatrix} = \alpha_3 \begin{bmatrix} 2 \\ 3 \\ 1 \\ 0 \\ 1 \end{bmatrix} + c \begin{bmatrix} 0 \\ 0 \\ 0 \\ 1 \\ 0 \end{bmatrix} \tag{33}$$

If Equation (21) opens to a Taylor series around $\varepsilon = 0$, the equation

$$\Psi = (1 - \varepsilon\alpha_1)\overline{\Psi}, \; x = (1 - \varepsilon\alpha_2)\overline{x}, \; y = (1 - \varepsilon\alpha_3)\overline{y}, \; U_\infty = (1 - \varepsilon\alpha_4)\overline{U}_\infty, \; T = (1 - \varepsilon\alpha_5)\overline{T} \tag{34}$$

has been found. Assuming that. $d\Psi = \overline{\Psi} - \Psi, dx = \overline{x} - x, dy = \overline{y} - y, dU_\infty = \overline{U}_\infty - U_\infty$, after drawing ε from the above equation, if all expressions are equalized, the following infinitesimal equations are written.

$$\frac{d\Psi}{2\Psi} = \frac{dx}{3x} = \frac{dy}{y} = \frac{dT}{cT} = \frac{dU_\infty}{U_\infty} \tag{35}$$

By integrating the terms in the above equation in groups of two, first the similarity variable then the streamline, temperature and uniform velocity of the fluid from the integral constants are found in order as follows.

$$\xi = x^{-1/3} y, \; f(\xi) = x^{-2/3}\Psi, \; \theta(\xi) = x^{-k/3}T, \; h(\xi) = x^{-1/3}U_\infty \tag{36}$$

Notice here that $\xi = \xi(x, y)$ and $U_\infty(x) = x^{1/3}h(\xi)$. However, $h(\xi)$ should not have a dependency on y since it should be $U_\infty = U_\infty(x)$. Hence $h(\xi)$ can be taken as constant or without loss of generality as $h = 1$. From here it becomes $U_\infty = x^{1/3}$. It also turns out that the reference velocity we defined in Equation (23) is $= x^{-1/3}U_\infty^*$. Now, using the computed similarity variable and functions, we can arrive at the momentum boundary layer equation reduced to the following ordinary differential form.

$$f''' \left(\frac{1 - n|\mathrm{Wi}\,f''|^n \left(1 + |\mathrm{Wi}\,f''|^n\right)^{-1}}{1 + |\mathrm{Wi}\,f''|^n} \right) + \frac{1}{3}\left(2ff'' - f'^2\right) + 1 = 0 \tag{37}$$

The conditions given in Equation (27) should also be transformed in terms of similarity function.

$$\begin{aligned} \Psi_y(x,0) = 0 &\rightarrow f'(0) = 0, \\ \Psi_y(x,\infty) = U_\infty &\rightarrow f'(\infty) = 1, \\ \Psi_x(x,0) = 0 &\rightarrow f'(0) = 0, \\ \Psi_{yy}(x,\infty) = 0 &\rightarrow f''(\infty) = 0. \end{aligned} \tag{38}$$

A shear stress and hence drag force will arise on the plate as a result of momentum transfer from the viscous fluid. Therefore, although the calculation of the shear stress on the plate surface is important, the below can be expressed by using the similarity transformations we have derived so far and the dimensionless version of Equation (13).

$$\sqrt{\mathrm{Re}}\, C_f = \left(1 + |\mathrm{Wi}\,f''(0)|^n\right)^{-1} f''(0) \tag{39}$$

Here $C_f = \tau_{x^*y^*}/\rho V^2$ is the dimensionless surface friction coefficient. The thermal boundary layer equation is reduced to the following ordinary differential equation, similar to that related to momentum.

$$\theta'' + \frac{\Pr}{3}\left(2f\,\theta' - c\,f'\,\theta\right) = 0 \tag{40}$$

The following

$$\theta(0) = x^{-c/3} \tag{41}$$

is obtained from the transformation of the temperature condition on the plate. The value of the constant c, which we left arbitrarily before, must be taken zero for the above transformation to occur, so

$$\theta(0) = 1 \tag{42}$$

is found. The temperature condition at infinity is easily found in terms of the similarity function as follows:

$$\theta(\infty) = 0 \qquad (43)$$

Thermal boundary layer equation given in Equation (40) turns into the following form with $c = 0$.

$$\theta'' + \frac{2\,\mathrm{Pr}}{3} f\,\theta' = 0 \qquad (44)$$

When the fluid and the plate are at different temperatures, a continuous heat transfer will occur between each other. It is determined by the dimensionless Nusselt number which convection and conduction mechanisms will be more prominent in the heat transfer process. Therefore, the Nusselt number is briefly defined as the ratio of the amount of heat transferred by convection to that of the conduction. As the Nusselt number increases, the effect of convection mechanism becomes dominant in total heat transfer. In analytical terms, it is the expression related to the temperature gradient at the surface given below.

$$Nu_{hL/k} = -\sqrt{\mathrm{Re}} \left. \frac{\partial T}{\partial y} \right|_{y=0} \qquad (45)$$

It is reduced to the form of the local Nusselt number as

$$Nu_x = -\sqrt{\mathrm{Re}}\,\theta'(0) \qquad (46)$$

in terms of similarity functions. It should be noted that the Nusselt number given by Equation (45) is defined as $Nu_x = hx^{*\frac{1}{3}}/k$ in the similarity transformation procedure.

5. Numerical Study

In this section, numerical solution of Equations (37) and (44) will be obtained under the boundary conditions of Equation (38), (42) and (43). As a numerical solution approach, bvpsuite2.0 (Wurm 2016) package developed for Matlab environment was used. Developed for nonlinear and implicit boundary value problems, the bvpsuite2.0 package can also generate valid numerical solutions for problems with singularities in integral boundaries (Fallahpour *et al*. 2018). The algorithm uses a collocation method (Weinmuller 1986) based on the principle of providing the differential equation of piecewise polynomial functions at collocation points

such as Gauss-Legendre and Lobatto. Integral interval is divided into equal solution intervals and 2-point Gaussian collocation is applied to each interval. A predictive solution and dense mesh structure were needed because the problem under consideration was nonlinear and rapidly changing. "Fast frozen Newton method" was used for the solution of nonlinear algebraic equation system resulting from polynomial collocation. For a successful convergence, the Newtonian solution, i.e., $Wi = 0$, was given to the algorithm as the estimated initial values and by increasing the Cross-fluid parameters gradually, each solution was used as the predictive solution of the next. A factor affecting the convergence of colocation methods is the density of the solution points, or in other words, the mesh structure. Another feature of the program used is that the number of mesh points can be increased by dividing the gaps into two if needed, thanks to a special mesh adaptation algorithm. In all numerical procedures, the initial mesh structure consists of 31 points equidistant from each other, for example, there are 526 points in the mesh structure where error tolerances are provided for $Wi = 1, m = 0.5$ and $Pr = 1$ values. In this way, in cases where the user initially suggests insufficient mesh points, termination of the program and the repeated intervention of the user is prevented. Incidentally, it should be noted that in both nonlinear solver and mesh adaptation, absolute and relative error tolerances are taken as $E_a = 10^{-9}$ and $E_r = 10^{-9}$, respectively.

In order to see the variations of all boundary layer variables with their derivatives, the system of equations should be reduced to the first order ordinary differential equation system. For this, the following new variables are defined.

$$f = f_1, f' = f_2, f'' = f_3, \theta = f_4, \theta' = f_5 \qquad (47)$$

In terms of these variables, Equations (37) and (44) are reduced to the following system.

$$f_1' = f_2,$$
$$f_2' = f_3$$
$$f_3' = -\left(1 + \frac{2f_1 f_3 - f_2^2}{3}\right)\left(\frac{1 - n\left|\mathrm{Wi}\,f_3\right|^n\left(1 + \left|\mathrm{Wi}\,f_3\right|^n\right)^{-1}}{1 + \left|\mathrm{Wi}\,f_3\right|^n}\right)^{-1} \quad (48)$$
$$f_4' = f_5,$$
$$f_5' = -\frac{2}{3}\Pr f_1 f_5$$

The conditions that these equations are subject to are given below.

$$f_2(0) = 0,\ f_2(\infty) = 1,\ f_3(\infty) = 0,\ f_4(0) = 1,\ f_4(\infty) = 0. \quad (49)$$

In addition to the above conditions, the condition of the streamline function can be zero on the plate, i.e., $f_1(0) = 0$. Although the number of boundary conditions more than necessary causes the system to be overdetermined, $f_3(\infty) = 0$ condition was not used in numerical solutions, but it was checked that this condition was also fulfilled. Finally, the shear stress and Nusselt number in terms of new variables defined by Equation (47) turn into the following states.

$$\sqrt{\mathrm{Re}}\,C_f = \left(1 + \left|\mathrm{Wi}\,f_3(0)\right|^n\right)^{-1} f_3(0)\ \text{ and } Nu_x = -\sqrt{\mathrm{Re}}\,f_5(0) \quad (50)$$

6. Results and Discussion

In this section, the data of the numerical results will be plotted and the boundary layer behaviour will be observed with the change of dimensionless fluid parameters. Before proceeding to the interpretation of the graphs, it should be stated that, by definition, the fluid velocities in the boundary layer are related to the derivatives of the stream function with respect to the space and the equivalent of this in the solved equation system is $f'(\zeta)$.

In Figure 3, the change of $f'(\zeta)$ function associated with the momentum velocity boundary layer for different n values according to the similarity variable ζ is given. When the Cross-fluid formula given in Equation (3) is examined, the apparent viscosity of the fluid decreases with increasing deformation rates, while the increase in fluid parameters will show a multiplier effect on this decrease. This observation is consistent with the increase in fluid

velocity and the formation of a thinner boundary layer against increasing n values when Figure 3 is examined. A similar situation occurs in Figure 4 with the increase in the Weissenberg number directly related to the other non-Newtonian fluid parameter λ. From Figure 4, it can be seen that the fluid catches the free flow rate faster in increasing Wi numbers after touching the plate. As this behaviour indicates less friction, it should be said that at sufficiently large Wi numbers the flow will completely turn into ideal flow and the boundary layer will disappear.

In Figure 5, the shear stress applied by the fluid resulting from the momentum transfer to the plate is examined in terms of similarity functions, see Equation 39, for increasing values of Wi and n. When examining the momentum boundary layer, it was stated that the increase in both non-Newtonian fluid properties would bring the flow closer to the ideal state. Consistent with this, since the shear stress on the plate is zeroed in the ideal case, it is obvious that the shear stress will decrease for these increasing values. However, exceptional cases occur with $Wi < 1$ curves. This phenomenon can be explained by the coefficients Wi^n in our equations as a result of the nondimensionalization procedure we apply. Note that when $Wi < 1$, Wi^n will decrease for increasing n values. The effect of the Weissenberg number on shear stress will dominate as an increase up to a certain value of n. After this threshold is passed, the effect of deformation rate will become prominent and will reduce shear stress.

In Figure 6, against the increasing n values, the change of the similarity function θ related to the temperature of the fluid was observed through the similarity variable ζ. It should first be reminded that 1 in the y coordinate of the graph corresponds to the plate temperature without dimension and 0 to the free flow temperature. For this reason, as it moves on the plate in the vertical direction, i.e., $\zeta > 0$, the dimensionless fluid temperature changes faster between these limit temperatures in response to increasing n values. This behaviour can be interpreted as the fluid will reach the free flow temperature T_∞^* more quickly along the vertical coordinate after it contacts the plate. Therefore, a narrower thermal boundary layer will be

encountered for increasing n values. In Figure 7, the similarity function θ along the ζ coordinate is expressed in response to increasing Weissenberg numbers. In the same conditions, a fluid with a larger Wi reaches a dimensionless uniform temperature T_∞ or $\theta(\infty) = 1$ much faster in the vertical direction and thickening of the thermal boundary layer is prevented. Note that the effect of the increase in Wi and n values on the thermal boundary layer for the part up to here is parallel with the momentum boundary layer. The change of the similarity function θ according to the Prandtl number, which is the ratio of momentum diffusion to thermal dissipation, is given in Figure 8. For increasing Prandtl numbers, the effect of momentum transfer becomes prominent in the change of temperature of the fluid and the temperature gradient in the vertical direction increases. Thus, this increases in the rate of change of fluid temperature leads to a narrower thermal boundary layer. In addition, the Prandtl number and the thickness of the momentum and thermal boundary layers can be interpreted. Therefore, for a constant momentum boundary layer thickness, increasing Prandtl numbers cause thinning in the thermal boundary layer, as seen in Figure 8. For example, molten metal streams have low Prandtl numbers, i.e., $Pr \ll 1$, and accordingly, have a much thicker thermal boundary layer than the momentum boundary layer. When looking at such a situation from the heat transfer level, it can be said that the conduction mechanism is more dominant than the convection, although there is fluid motion.

High Nusselt numbers indicate that the convection mechanism is much more effective than conduction in net heat transfer between media. The effects that cause the unit mass of the fluid to displace faster on the plate will increase the convection and heat transfer. Therefore, fluid thinning facilitates transport and increases the Nusselt number. In the light of this information, Nusselt numbers versus n curves are plotted for different Weissenberg numbers in Figure 9. In the analyses regarding the momentum boundary layer, it was stated that the increase in Wi and n values thin the fluid. Therefore, it can be seen from Figure 9 that the increase in both

values increases the transport and increases the Nusselt number. It is observed that the effect of the increase in the n parameter becomes more prominent with the increase in the number of Wi and increases the Nusselt number more rapidly. Finally, for this graph, it should be said for values of $Wi < 1$, that the exception encountered in shear stress, i.e., the Wi^n effect, leads to decreasing Nusselt numbers for increasing n values.

Reminding that the collocation points are taken between two adjacent mesh points, the approximate error of $f'(\zeta)$ solution for $m = 0.5$ and $Wi = 1$ in Figure 10 is given in total 2194 mesh and collocation points. Initially, it consisted of 51 points equidistant from each other for the mesh structure, while the desired error tolerance was achieved at 732 points thanks to the mesh adaptation. In addition, when two Gaussian collocation points are added to each interval, the solution is calculated at 2194 points in total. Accordingly, if attention is paid, in the figure the error is high in the starting regions where the function changes rapidly, while it decreases in the following points. Detailed theoretical information for the approximate error estimation used here can be found in (Kitzhofer *et al.* 2007).

7. Conclusions

Within the scope of this study, a shear thinning fluid was expressed mathematically with the Cross fluid formula and its boundary layer flow over the stationary plate was investigated. The fluid was considered to have a uniform velocity and temperature before contacting the constant temperature plate. Since fluid and plate are considered as environments with different temperatures, parts related to heat exchange were added to the analysis. Considering the boundary layer assumptions, the equations governing the physical process are extracted with boundary conditions in partial differential form without dimensions. It has been shown that the direct dimensionless Weissenberg number and n the power-law constant specific to the Cross-fluid model are responsible for the momentum boundary layer equation. For the thermal boundary layer

equation, it was expressed analytically that the effect of these parameters came indirectly depending on the fluid velocities and that the main dimensionless parameter was the Prandtl number. Then, the symmetries of the differential equations were calculated in order to reduce them to ordinary differential form, which is more suitable for numerical solutions. By using these symmetries, it has been shown that partial differential form equations and their conditions are successfully transformed into ordinary differential equations in terms of similarity functions. In addition, the shear stress and Nusselt numbers on the plate, which are important for applied sciences and engineering, are expressed in terms of similarity functions. The sbvp2.0 package based on polynomial collocation methods developed for Matlab environment was used to solve the final equations in ordinary form. The changes of momentum and thermal boundary layer thicknesses were analysed under the influence of parameters specific to the Cross-fluid formula by means of graphs drawn using the data obtained from the numeric scheme. The effects of the same parameters on the changes in shear stress and Nusselt number were interpreted again through graphs. When the critical analytical expressions of the study are examined, it is mentioned in the related graphics that the numerical results are logically appropriate.

The critical results specific to the Cross-fluid model from the framework of non-Newtonian fluid mechanics are summarized below.

- The increase in dimensionless Weissenberg number and n power-law coefficient, which are inversely proportional to the apparent viscosity of the cross fluid, thin the fluid as well as narrow the boundary layer and bring the flow closer to the ideal frictionless flow.
- Similarly, as the Weissenberg number and n values increase, the temperature gradient on the plate becomes very large, so the thermal boundary layer becomes thinner and the change in fluid temperature occurs very quickly. This increase brings the system closer to the ideal state where the fluid has a continuous uniform temperature, as in the momentum boundary layer.
- The shear stress applied by the fluid to the plate decreases with increasing Weissenberg number and n value and the flow becomes less viscous.
- The Nusselt number increases as a result of the heat transfer efficiency with increased convection according to the conduction in the fluid versus the increasing Weissenberg number and n value.

Finally, for stiff equations such as boundary layer equations, where change occurs very quickly in a narrow region, the sbvp2.0 package, where we can control more variables than Matlab's bvp4c command, but requires less user intervention after running, may be preferred. Especially despite the use of not very good predictive initial conditions and infrequent mesh structure, when two Gaussian collocation points and the algorithm's mesh adaptation is used, numerical procedures are completed quickly and successfully.
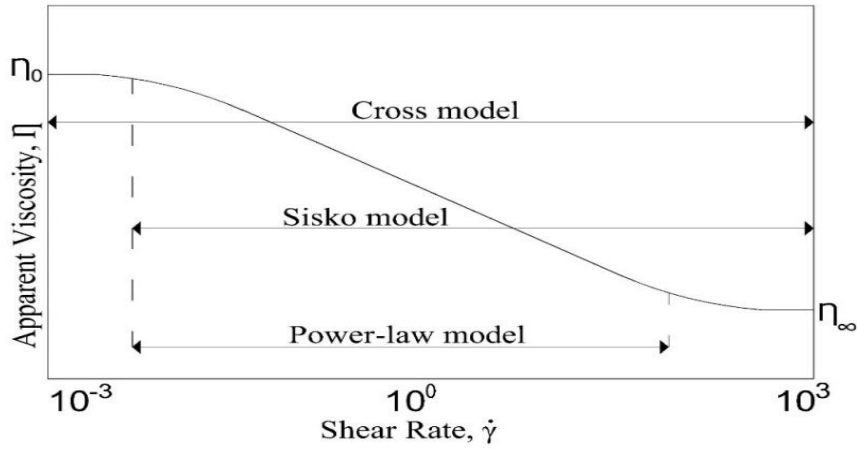
Figure 1. Representative schematic view of an apparent viscosity varying with increasing shear rate and confirming zones by non-Newtonian models
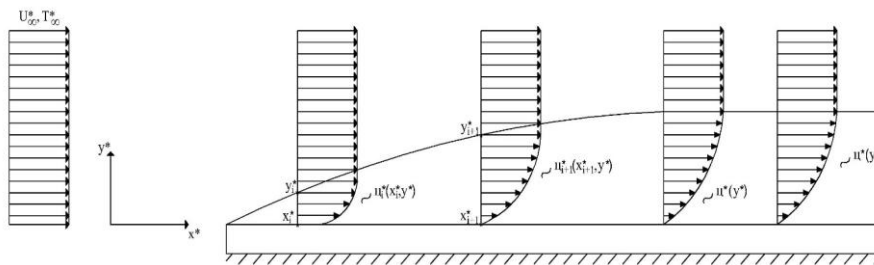

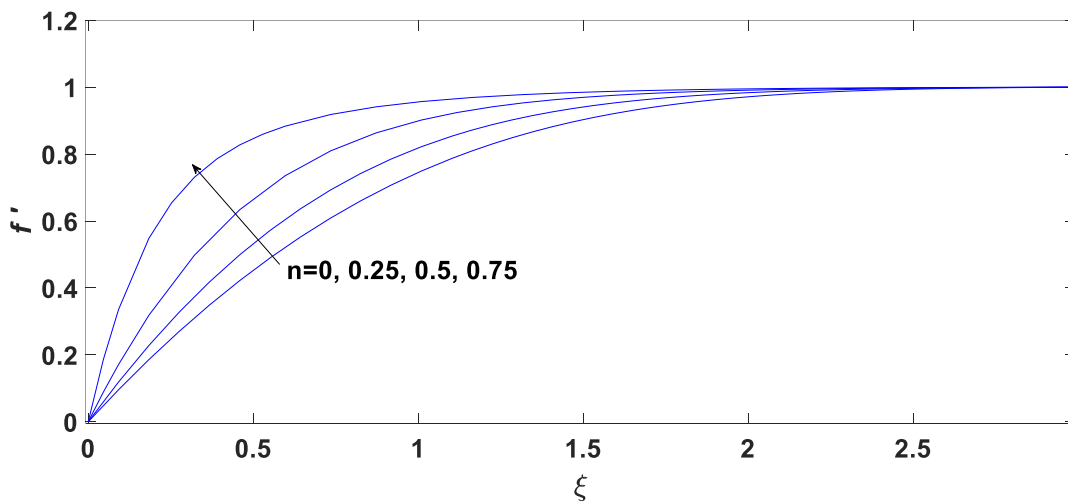**Figure 2.** Physical description of a boundary layer flow over a flat plate

Figure 3. Variations of the first derivative of the similarity function f with the similarity variable ξ for Various power-law index n $(\text{Wi} = 1)$
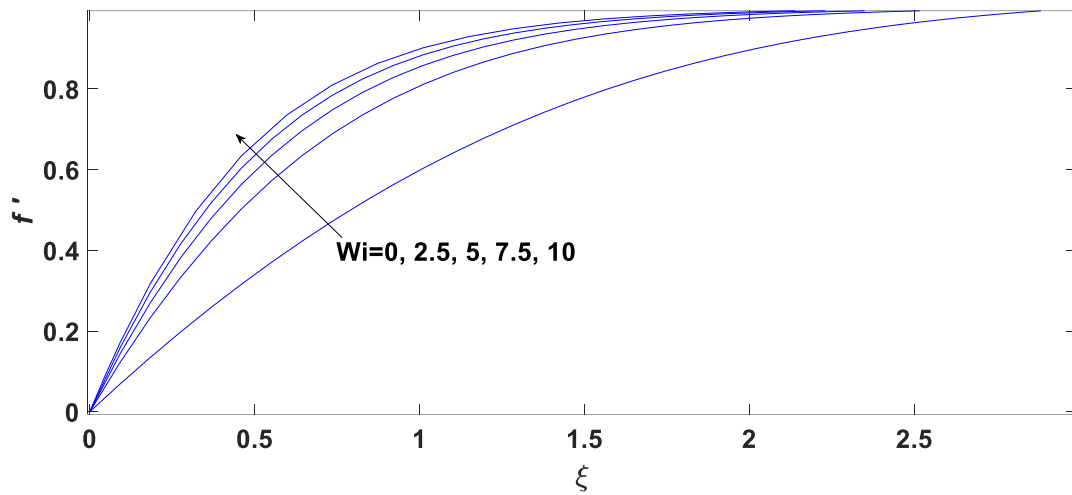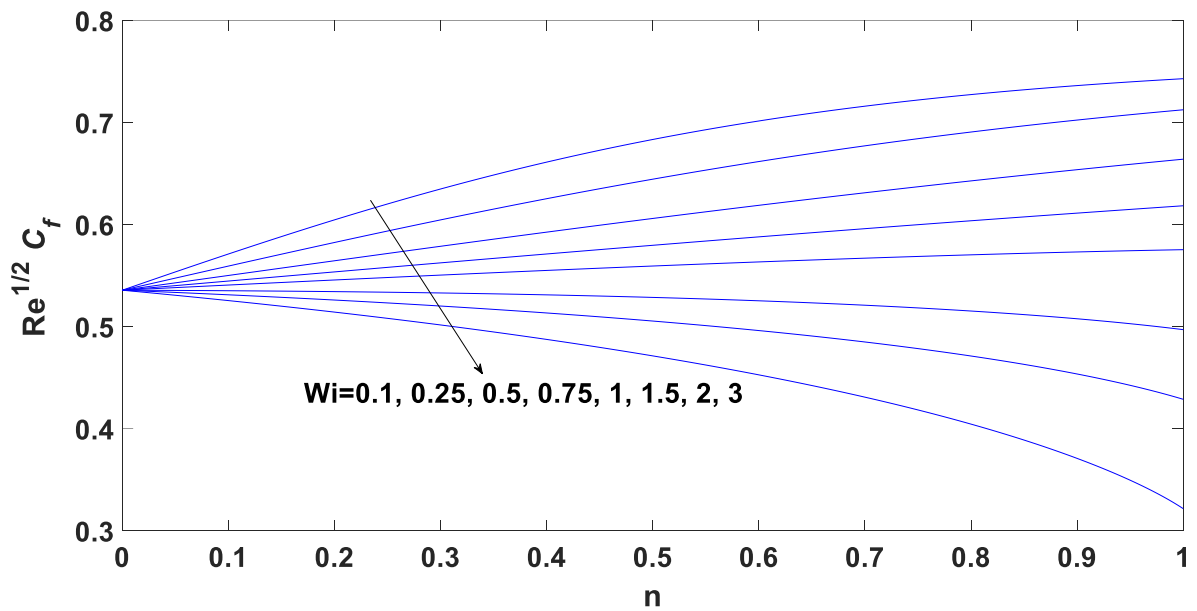
Figure 4. Variations of the first derivative of the similarity function f with the similarity variable ξ for various Weissenberg numbers ($n = 0.5$)

Figure 5. Variations of the dimensionless shear Stress with the power-law index n for various Weissenberg numbers
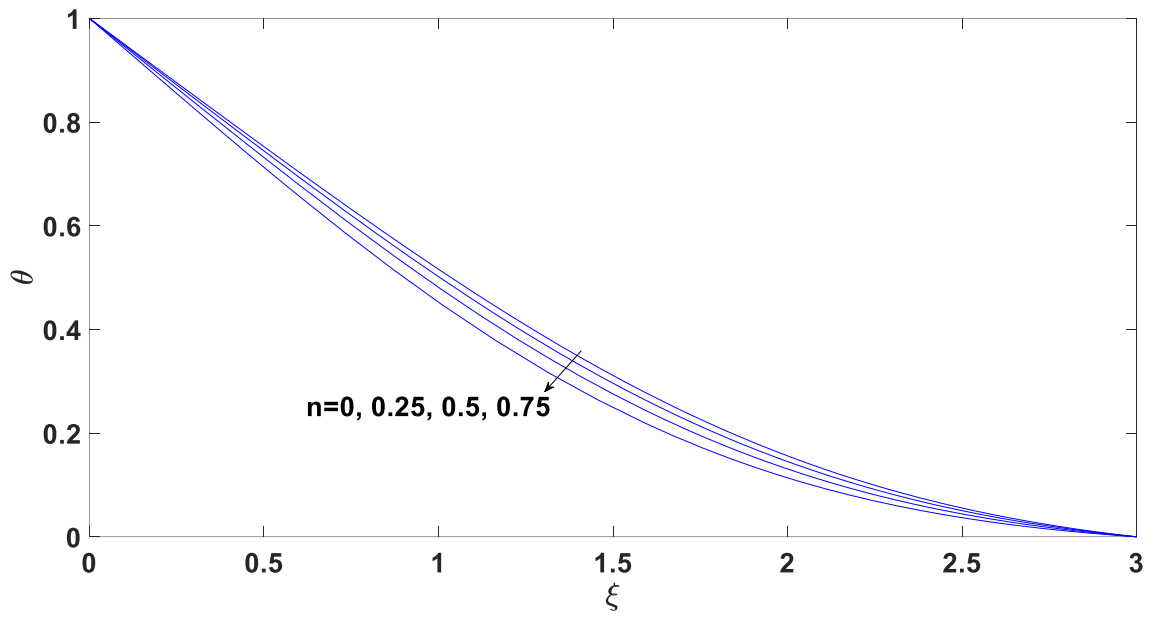
Figure 6. Variations of the dimensionless fluid temperature with the similarity variable ξ for various power-law index n ($\text{Wi} = 1, \text{Pr} = 1$)
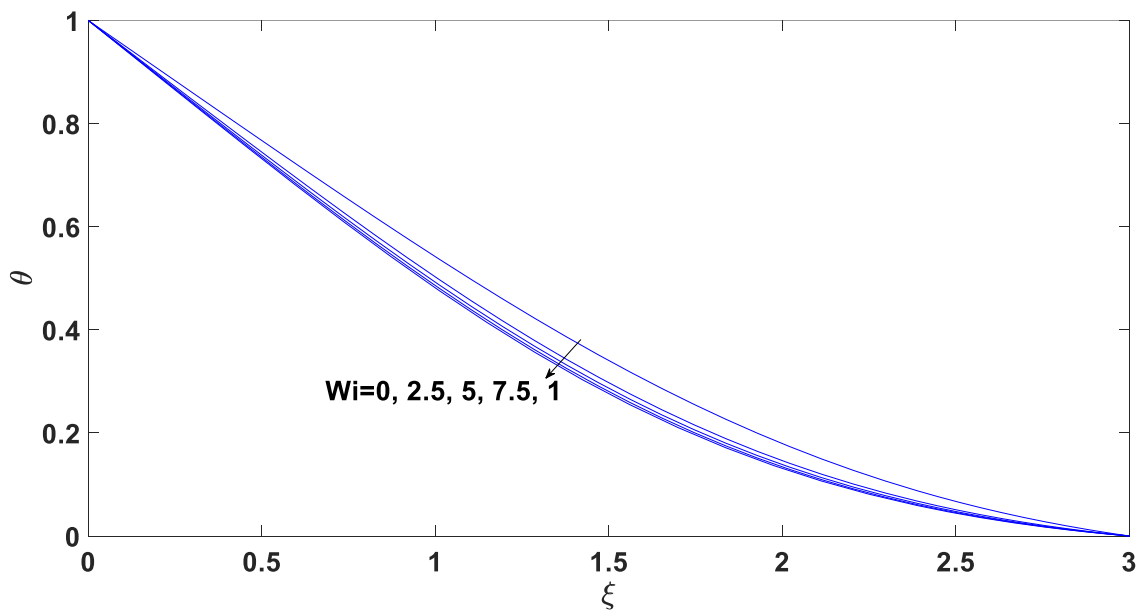

Figure 7. Variations of the dimensionless fluid temperature with the similarity variable ξ for various Weissenberg numbers ($n = 0.5, \text{Pr} = 1$)
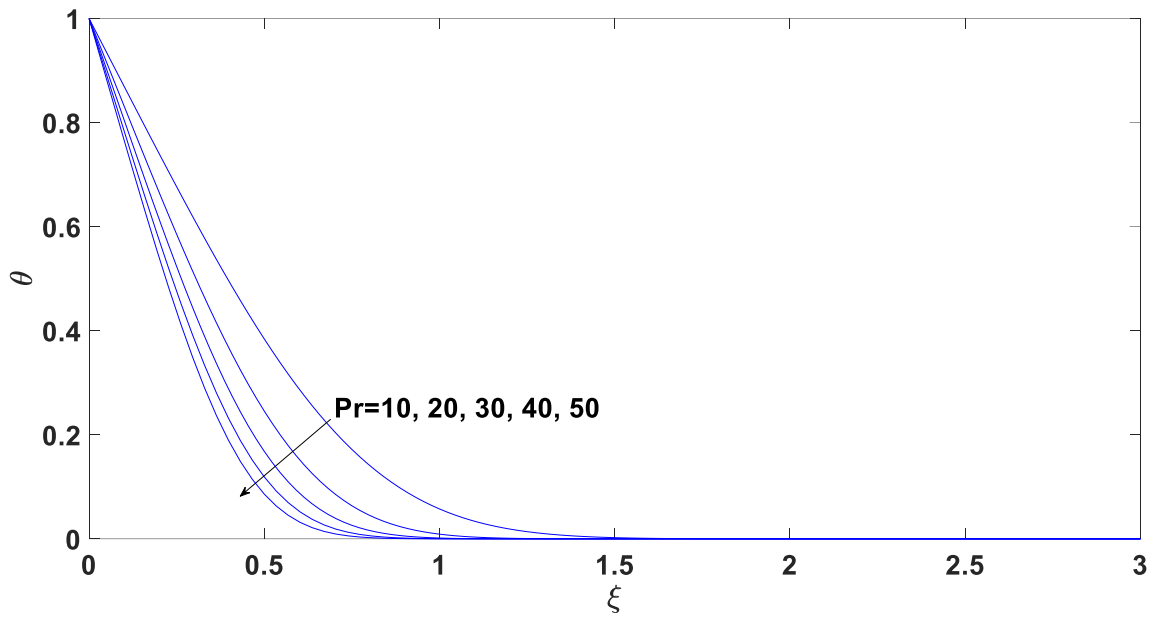
Figure 8. Variations of the dimensionless fluid temperature with the similarity variable ξ for various Prandtl numbers ($Wi = 1, n = 0.5$)
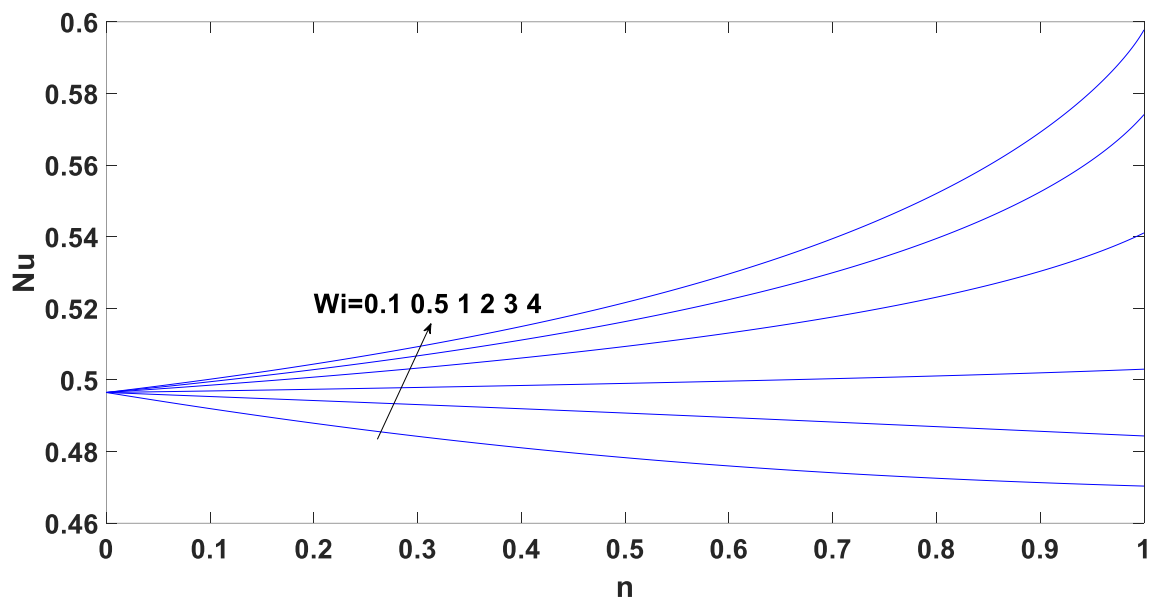

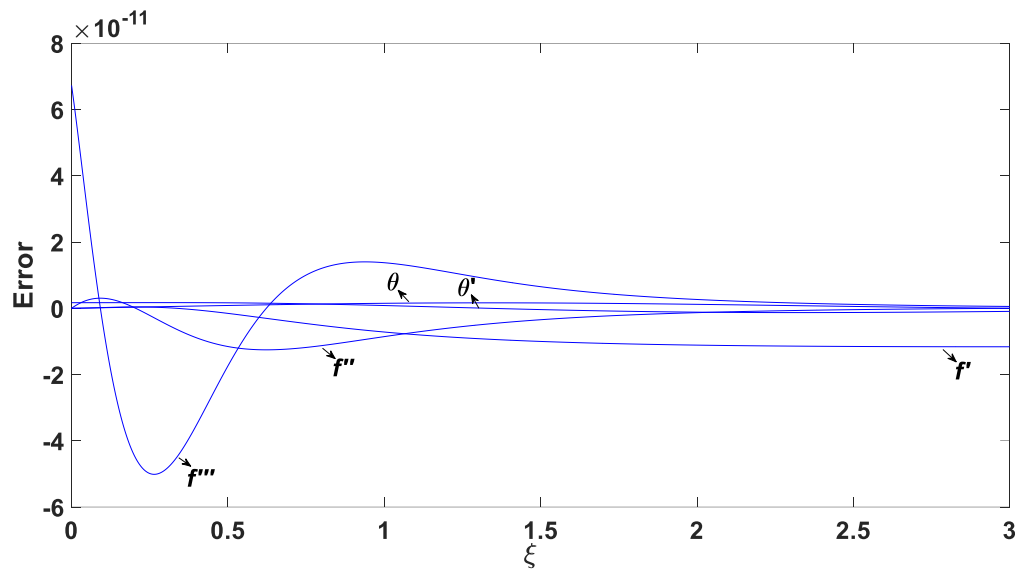**Figure 9.** Variations of the Nusselt number with the power-law index n for various Weissenberg numbers($Pr = 1$)

Figure 10. Approximate errors of a numerical solution ith respect to similarity functions and their derivatives

8. References

Aksoy, Y., Hayat, T., Pakdemirli, M., 2012, Boundary layer theory and symmetry analysis of a Williamson fluid, *Zeitschrift für Naturforschung A*, **67a(6-7)**, 363-368.

Aksoy, Y., Pakdemirli M., Khalique, C. M., 2007, Boundary layer equations and stretching sheet solutions for the modified second grade fluid, *International Journal of Engineering Science*, **45(10)**, 829-841.

Bird, R. B., 1976, Useful Non-Newtonian models, *Annual Review of Fluid Mechanics*, **8**, 13-34.

Bluman, G. W., Kumei, S., 2013, *Symmetries and differential equations*. Springer Science & Business Media, NY, 413.

Cross,M. M., 1965, Rheology of Non-Newtonian Fluids: A new Flow Equation For Pseudoplastic Systems, *Journal of Colloid Science*, **20(5)**, 417-437.

Değer, G., Pakdemirli, M., Aksoy, Y., 2011, Symmetry Analysis of Boundary Layer Equations of an Upper Convected Maxwell Fluid with Magnetohydrodynamic Flow, *Zeitschrift fur Naturforschung A-Journal of Physical Sciences*, **66(5)**, 321-328.

Fallahpour,M., Mckee,S., Weinmüller, E. B., 2018, Numerical simulation of flow in smectic liquid crystals, *Applied Numerical Mathematics*, **132**, 154-162.

Galindo-Rosales, F. J., Rubio-Hernandez, F. J., Sevilla, A., 2011, An apparent viscosity function for shear thickening fluids, *Journal of non-Newtonian Mechanics*, **166(5-6)**, 321-325.

Hayat, T., Pakdemirli, M., Aksoy, Y., 2013, Similarity solutions for boundary layer equations of a Powel-Eyring fluid, *Mathematical and Computational Applications*, **18(1)**, 62-70.

Iftikhar, N., Riaz, M. B., Awrejcewicz, J., Akgül, A., 2021, Effect of magnetic field with parabolic motion on fractional second grade fluid, *Fractal and Fractional*, **5(4)**, 163.

Javaid, M., Tahir, M., Imran, M., Baleanu, D., Akgül, A., Imran, M. A., 2022, Unsteady flow of fractional Burger's fluid in a rotating annulus region with power-law kernel, *Alexandria Engineering Journal*, **61(1)**, 1727.

Javed, F., Riaz, M. B., Iftikhar, N., Awrejcewicz, J., Akgül, A., 2021, Heat and mass transfer impact on differential type nanofluid with carbon nanotubes: a study of fractional order system, *Fractal and Fractional*, **5(4)**, 231.

Kitzhofer, G., Koch, O., Lima, P., Weinmüller, E., 2007, Efficient numerical solution of the density profile equation in hydrodynamics, *Journal of Scientific Computing*, **32(3)**, 411-424.

Morrison, F. A., 2001, Understanding Rheology. Oxford University Press, New York ABD , 446.

NA, T. Y., 1994, Boundary layer flow of Reiner-Philippoff fluids, *International Journal of Non-Linear Mechanics*, **29(6)**, 871-877.

Pakdemirli,M., Aksoy Y., Yürüsoy, M., Khalique M., 2008, Symmetries of boundary layer equations of power-law fluids of second grade, *Acta Mechanica Sinica*, **24(6)**, 661-670.

Pakdemirli,M., HAYAT, T., Aksoy Y., 2013, Group-theoretic approach to boundary layer equations of an oldroy-B fluid, *Zeitschrift für Naturforschung A*, **68(12)**, 785-790.

Raju,K. V. S. N., Krishna,D., Rama Devi, G., . Reddy, P. J., Yaseen, M., 1993, Assessment of applicability of Carreau, Ellis, and Cross models to the viscosity data of resin solutions, *Journal of Applied Polymer Science*, **(48)**, 2101-2112.

Riaz, M. B., Rehman, A., Awrejcewicz, J., Akgül, A., 2021, Power-law kernel analysis of mhd Maxwell fluid with ramped boundary conditions: transport phenomena solutions based on special functions, *Fractal and Fractionals*, **5(4)**, 248.

Riaz, M. B., Abro, K. A., Abualnaja, K. M., Akgül, A., Rehman A., Abbas, M., Hamed, Y. S., 2021, Exact solutions involving special functions for steady convective flow of magnetohydrodynamic second grade fluid with ramped conditions, *Advances in Difference Equations*, **2021(1)**, 1-14.

Sarı, G., Pakdemirli, M., Hayat, T., Aksoy, Y.,2012, Boundary layer equations and Lie group analysis of a Sisko fluid, *Journal of Applied Mathematics*, doi: 10.1155/2012/259608.

Schlichting, H., Gersten K., 2017, *Boundary-Layer Theory*. Berlin, Springer, Heidelberg, Berlin, 805.

Sisko, A. W., 1958, The flow of lubricating greases, *Industrial & Engineering Chemistry,* **50(12)**, 1789-1792.

Sunthrayuth, P., Alderremy, A., Aly, S., Shah, R., Akgül, A., 2021, Exact analysis of electro-osmotic flow of Walters'-B fluid with non-singular kernel, *Pramana*, **95(4)**, 1-10.

Wan Nik, W.B., Ani, F. N., Masjuki, H. H., Eng Giap S. G., 2005, Rheology of bio-edible oils according to several rheological models and its potential as hydraulic fluid, *Industrial Crops and Products*, **22(3)**, 249-255.

Weinmuller, E. B., 1986, Collocation for singular boundary value problems of second order, *SIAM journal on numerical analysis*, **23(5)**, 1062-1095.

Williamson, R. V., 1929, The Flow of Pseudoplastic Materials, *Industrial & Engineering Chemistry*, **21(11)**, 1108-1111.

Wurm, S., At 2016, BVPsuite 2.0 a new version of a collocation code for singular BVPs in ODEs EVPs and DAEs, Ph.D. dissertation, TU, Wien, 110.

Yasuda,K., Armstrong,R. C., Cohen, R. E., 1981, Shear flow properties of concentrated solutions of linear and star branched polystyrenes, *Rheologica Acta*, **20**, 163-178.